SUPPLEMENTARY MATERIAL

Supplementary Table 1: Patient and aneurysm characteristics of the training and testing datasets.

Characteristics		Training Dataset	Testing Dataset
Population	US	1192	131
	EU	197	-
	SA	13	-
	FIN	71	64
	JAP	141	-
Patient	Age	57.1 [12-100] y	55.6 [25-81] y
	Sex	F=1037 (64%), M=396 (25%), U=181 (11%)	F=128 (66%), M=44 (22%), U=23 (12%)
	Multiplicity	M=438 (27%), S=1176 (73%)	M=51 (26%), S=144 (74%)
	Total	1614	195
Aneurysm	Size	6.7 [1.1-39.3] mm	7.5 [1.3-42.6] mm
	Blebs	Y=735 (31%), N=1660 (69%)	Y=95 (36%), N=171 (64%)
	Total	2395	266

Blebs: Y=yes, N=no. Sex: F=female, M=male, U=unknown. Multiplicity: M=multiple, S=single.

Supplementary Table 2: Bleb presence in aneurysms imaged with 3DRA and CTA.

Imaging Modality	Aneurysms with Blebs	Aneurysms without Blebs	P-Value
3DRA	68 (38%)	112 (62%)	1.0
CTA	29 (32%)	61 (68%)	
All	97 (36%)	173 (64%)	

The non-significant p-value of the Fisher's test in this 2x2 contingency table indicates that there is no significant difference in the presence of blebs depending on the imaging modality. This justifies the merging of the 3DRA and CTA data for the current study.

Supplementary Table 3: Hemodynamic and geometric characteristics associated with bleb development.

Characteristic	Variable	Aneurysms with blebs	Aneurysms without blebs	p-value	Adjusted p-value
		Mean ± SD	Mean ± SD		
Hemodynamics					
Inflow jet	Q (ml/s)	1.93 ± 0.85	0.57 ± 0.72	<0.01*	<0.01*
	ICI	1.23 ± 0.76	0.61 ± 0.73	<0.01*	<0.01*
Flow pattern	VE (cm/s)	9.31 ± 6.04	8.79 ± 6.73	<0.01*	<0.01*
	VD	1708 ± 1725	1579 ± 1396	0.85	1
	corelen (mm)	21.7 ± 25	12.5 ± 20.2	<0.01*	<0.01*
	podent	0.21 ± 0.15	0.17 ± 0.13	<0.01*	<0.01*
Wall shear stress pattern	WSSmax (dyn/cm^2)	384 ± 395	225 ± 205	<0.01*	<0.01*
	WSSmean (dyn/cm^2)	25.1 ± 19.9	20.9 ± 21.8	0.08	1
	MaxWSSnorm	6.98 ± 5.11	5.47 ± 5.37	<0.01*	<0.01*
	WSSnorm	0.47 ± 0.30	0.51 ± 0.34	<0.01*	<0.01*
	LSA (%)	49.9 ± 33.1	50.6 ± 33.5	0.37	1
	SCI	6.05 ± 7.45	4.14 ± 5.10	<0.01*	<0.01*
	OSImax	0.32 ± 0.11	0.25 ± 0.14	<0.01*	<0.01*
	OSImean	0.02 ± 0.02	0.01 ± 0.02	<0.01*	<0.01*
	nCrPoints	2.34 ± 1.02	1.55 ± 1.12	<0.01*	<0.01*
Geometry					
Size	Asize (mm)	8.1 ± 3.6	6.1 ± 4.1	<0.01*	<0.01*
	Nsize (mm)	4.9 ± 2.1	4.2 ± 2.2	<0.01*	<0.01*
	SR	2.43 ± 1.19	1.76 ± 1.26	<0.01*	<0.01*
	GAA (cm^{-1})	9.31 ± 8.08	21.8 ± 24.2	<0.01*	<0.01*
Elongation	AR	1.19 ± 0.62	0.90 ± 0.62	<0.01*	<0.01*
	VOR (mm)	9.83 ± 17.9	6.35 ± 15.1	<0.01*	<0.01*
	BF	1.34 ± 0.43	1.15 ± 0.41	<0.01*	<0.01*
Shape distortion	NSI	0.22 ± 0.05	0.20 ± 0.05	<0.01*	<0.01*
	CR	0.81 ± 0.11	0.76 ± 0.13	<0.01*	<0.01*
Irregularity	UI	0.19 ± 0.11	0.24 ± 0.13	<0.01*	<0.01*

The 'Adjusted p-value' column lists the p-values after adjustment for multiple testing using the Bonferroni method.

Supplementary Table 4: Variables considered for predictive modeling of bleb development from four different domains.

Domain	Variable	Meaning	Retained
Patient	Age	Patient age (years)	No
	Sex	Patient sex (F/M)	No
	Population	Patient population (US, EU, SA, FIN, JAP)	Yes
Aneurysm	Location	Aneurysm location (ACA,ACOM,BA,ICA,MCA,PCOM,PICA)	Yes
	Morphology	Aneurysm morphology (lateral/bifurcation)	Yes
	Multiplicity	Aneurysm multiplicity (single/multiple)	Yes
Hemodynamics	Q	Mean aneurysm inflow rate (ml/s)	Yes
	ICI	Inflow concentration index	Yes
	VE	Mean aneurysm velocity (cm/s)	No
	VD	Mean aneurysm viscous dissipation	No
	corelen	Total vortex core-line length	Yes
	podent	Proper orthogonal decomposition entropy	No
	WSSmax	Maximum wall shear stress	No
	WSSmean	Time-averaged mean wall shear stress	No
	MWSSnorm	Max normalized WSS (over vessel WSS)	Yes
	WSSnorm	Mean normalized WSS	No
	LSA	Percent of aneurysm area under low WSS	No
	SCI	Shear concentration index	No
	OSImax	Maximum oscillatory shear index	Yes
	OSImean	Mean oscillatory shear index	No
	nCrPoints	Time-averaged number of critical points in WSS field	Yes
Geometry	Asize	Aneurysm maximum size	Yes
	Nsize	Neck maximum size	No
	SR	Size ratio	Yes
	GAA	Gaussian curvature	Yes
	AR	Aspect ratio	Yes
	VOR	Volume to ostium ratio	Yes
	BF	Bottleneck factor	Yes
	NSI	Non-sphericity index	Yes
	CR	Convexity ratio	Yes
	UI	Undulation index	No

Supplementary Table 5: Summary of evaluation metrics for different ML predictive models obtained during repeated internal cross-validation.

Model	AUC Mean [max]	TPR Mean [max]	FPR Mean [min]	Misclassification Error Mean [min]
BG	0.79 [0.82]	0.76 [0.81]	0.34 [0.26]	0.30 [0.25]
RF	0.80 [0.84]	0.80 [0.85]	0.33 [0.25]	0.28 [0.24]
SVM	0.78 [0.82]	0.75 [0.84]	0.33 [0.19]	0.30 [0.24]
KNN	0.74 [0.79]	0.76 [0.82]	0.39 [0.31]	0.34 [0.27]
LR	0.76 [0.79]	0.76 [0.82]	0.35 [0.28]	0.32 [0.28]

Supplementary Table 6: Pair-wise statistical significance scores between RF (best model) and other ML models for different performance metrics evaluated on the external validation set.

Comparison	AUC (p-value)	Sensitivity (p-value)	Specificity (p-value)
RF vs. BG	<0.01*	<0.01*	0.75
RF vs. LR	<0.01*	0.02*	0.43
RF vs. KNN	<0.01*	0.04*	<0.01*
RF vs. SVM	0.04*	0.04*	0.27

The differences were computed using a t-test to evaluate the null hypothesis that there is no difference between models. Significant p-values ($p<0.05$) indicated with '*' imply that the performance of the RF model is indeed better than the other models according to the corresponding metric.

Supplementary Table 7: Performance measures for each ML model applied to the external testing dataset using a limited number of predictive variables.

Model	AUC	TPR	FPR	PPV	NPV	F1 Score	Balanced Accuracy	Misclassification Error
BG	0.70	0.78	0.54	0.48	0.78	0.59	0.62	0.37
RF	0.77	0.84	0.41	0.54	0.87	0.66	0.73	0.31
SVM	0.71	0.79	0.54	0.47	0.83	0.59	0.63	0.39
KNN	0.72	0.77	0.45	0.50	0.81	0.61	0.66	0.39
LR	0.66	0.61	0.45	0.43	0.72	0.50	0.58	0.43

AUC=area under the ROC curve. TPR=true positive rate (sensitivity or recall = number of true positives divided by all positives). FPR=false positive rate (1-specificity = number of false positives divided by all negatives). PPV=positive predictive value (precision = number of true positives divided by number of true and false positives). NVP=negative predictive value (=number of true negatives divided by the number of true and false negatives). F1=2*PPV*TPR/(PPV+TPR)=harmonic mean of precision and recall. Balanced accuracy=accuracy accounting for class imbalance (=(sensitivity + specificity)/2). Misclassification error=number of incorrect classifications divided by sample size.

Aneurysm Shape before Bleb Development

Previous studies have shown that aneurysm growth can occur in a global manner where the aneurysm enlarges everywhere at the same time or in a focalized growth where enlargement occurs in a relatively small region of the aneurysm and can result in the formation of blebs (see for example Machi P, Ouared R, Brina O, et al.[21]). Furthermore, this same study showed on a small longitudinal dataset that globally and focally growing aneurysms tend to have different flow conditions at baseline. As such, flow, geometric, and aneurysm characteristics that favor focal growth can help us identify aneurysms prone to develop blebs.

In the current study, the conditions prior to bleb development are approximated by virtually deleting the blebs in 3D vascular reconstructions (as explained in the Methods section and Suppl. Fig. 3). This approach assumes that when blebs develop, the rest of the aneurysm sac does not change substantially, which is consistent with a focalized growth. To support this hypothesis, four examples of growing aneurysms that have been followed longitudinally without treatment and exhibit focalized growth and bleb development are presented in Suppl. Fig. 1. The baseline geometries are displayed in red, and the follow-up geometries are rendered in transparent gray overlayed with the baseline. It can be seen that in these cases, the aneurysm sac remains largely unchanged except in the region of focalized growth. In case A, an incipient bleb grows while the rest of the sac does not change. In case B, a large bleb with a well-defined neck develops while the rest remains unchanged. In case C, the initial development of a bleb can be observed. In case D, a bleb develops on the side of the aneurysm while there is a small global enlargement of the aneurysm at the fundus (showing that the bleb develops faster than the overall growth of the sac). These cases provide support to the assumption that deleting the blebs while maintaining the rest of the aneurysm sac unchanged provides a reasonable approximation of the conditions prior to bleb formation. See for example Suppl. Fig. 3 which provides an example quite similar to Suppl. Fig. 1B. Nevertheless, this hypothesis should be further investigated with larger longitudinal dataset of growing aneurysms.

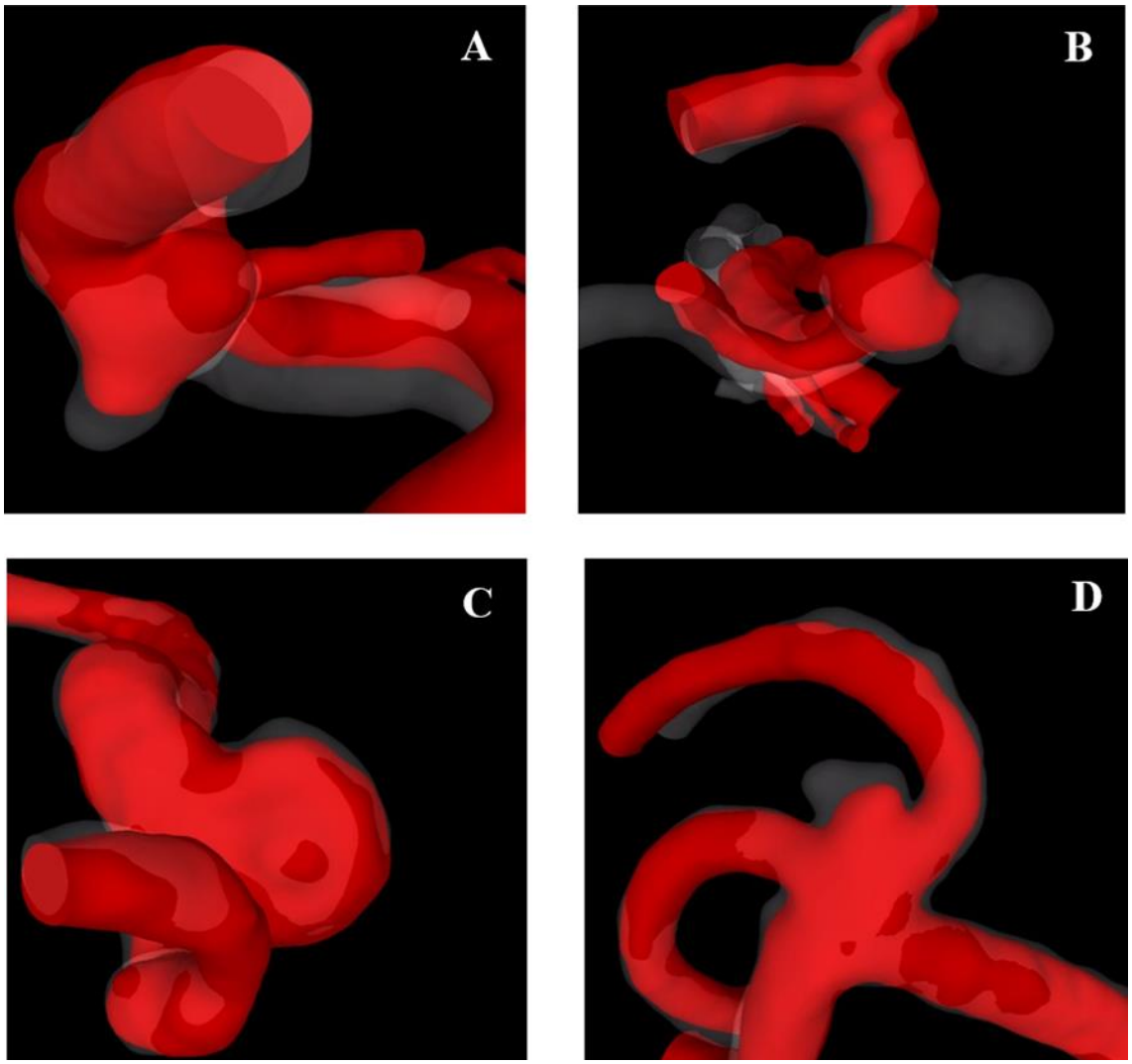

Supplementary Figure 1: Examples of four aneurysms that exhibited focalized growth and bleb development during follow-up without treatment. The red surface corresponds to the baseline vascular geometry, and the transparent gray surface corresponds to the vascular geometry at follow-up. Removal of the blebs in the follow-up geometry while maintaining the rest of the aneurysm geometry unchanged seems quite reasonable in these examples, thus providing support for the underlying assumption of the current study.

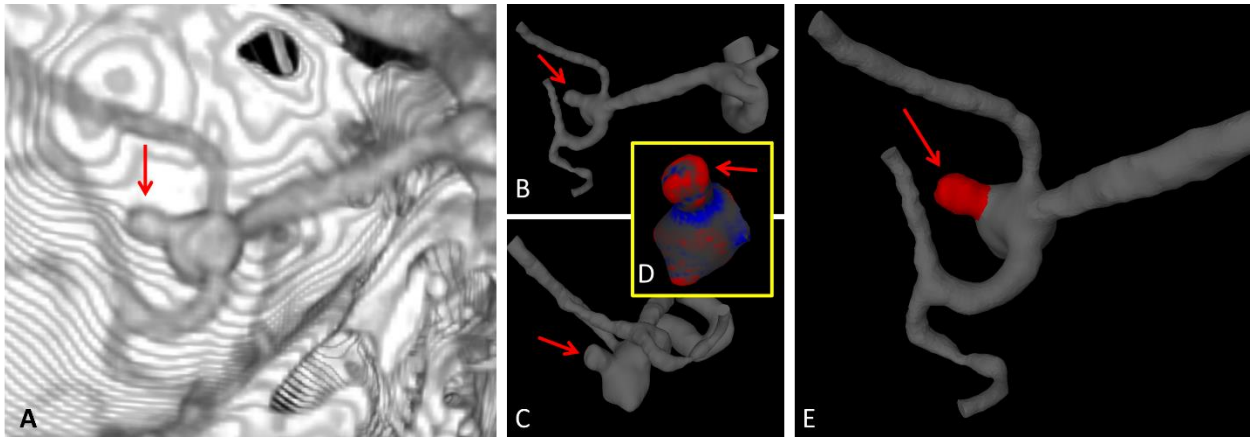

Supplementary Figure 2: Identifying and marking blebs. A: volume rendering of MCA bifurcation aneurysm with bleb (red arrow) imaged with CTA. B and C: reconstructed vascular model from two different viewpoints demonstrating the bleb (red arrows). D: curvature map of the aneurysm dome showing the bleb as a region of positive curvature (red) surrounded by a band of negative curvature (blue). E: bleb region interactively marked (painted) on the 3D vascular model.

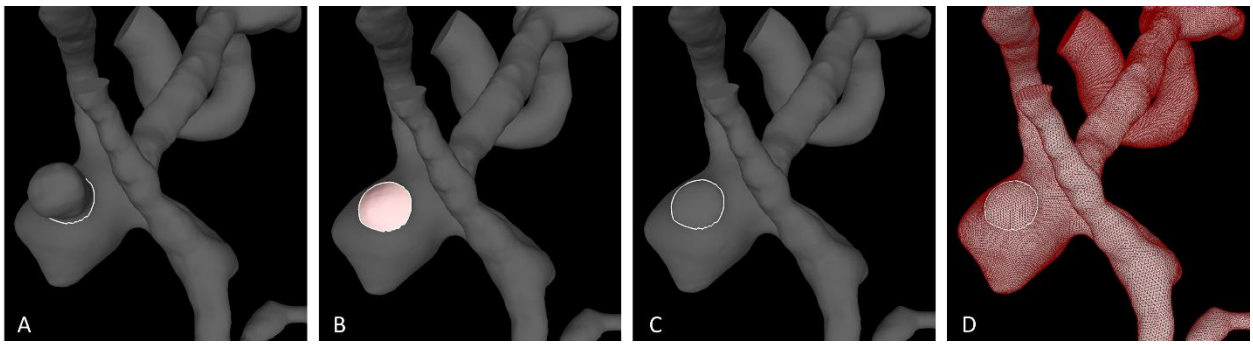

Supplementary Figure 3: Removing blebs to model aneurysm prior to bleb formation. A: vascular model with bleb (same aneurysm as in Suppl. Fig. 2). B: deletion of surface elements (triangles) in marked bleb region. C: re-triangulation of the vascular model to close the hole after bleb deletion. D: computational mesh used for CFD simulation of flow in aneurysm prior to bleb formation.

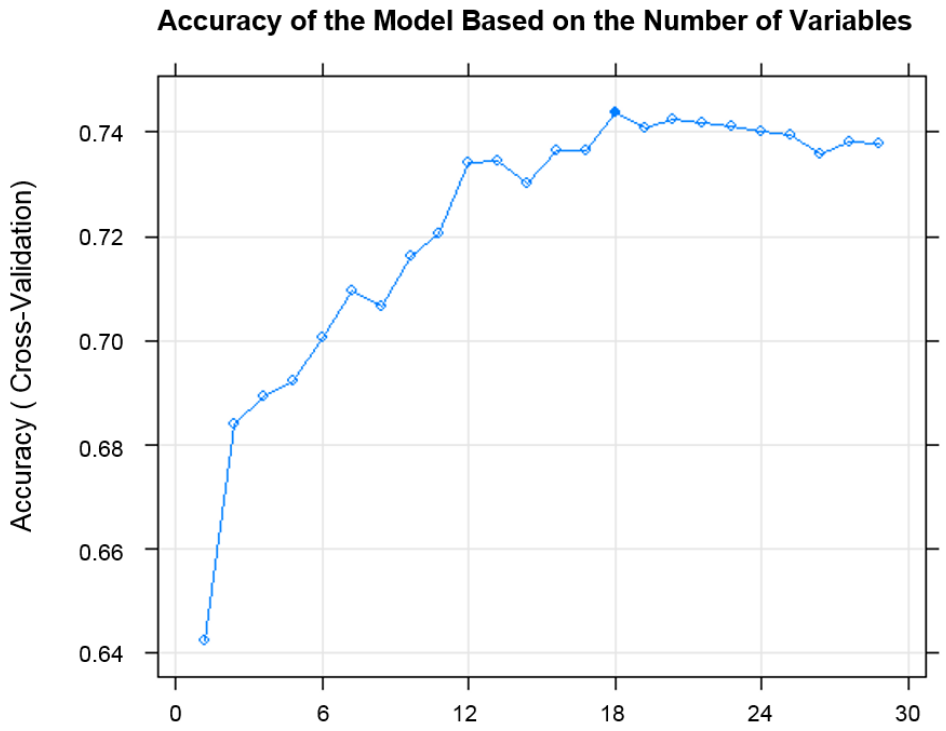

Supplementary Figure 4: Accuracy of ML models with different number of variables (in decreasing order of importance) during the 10-fold cross-validation process.

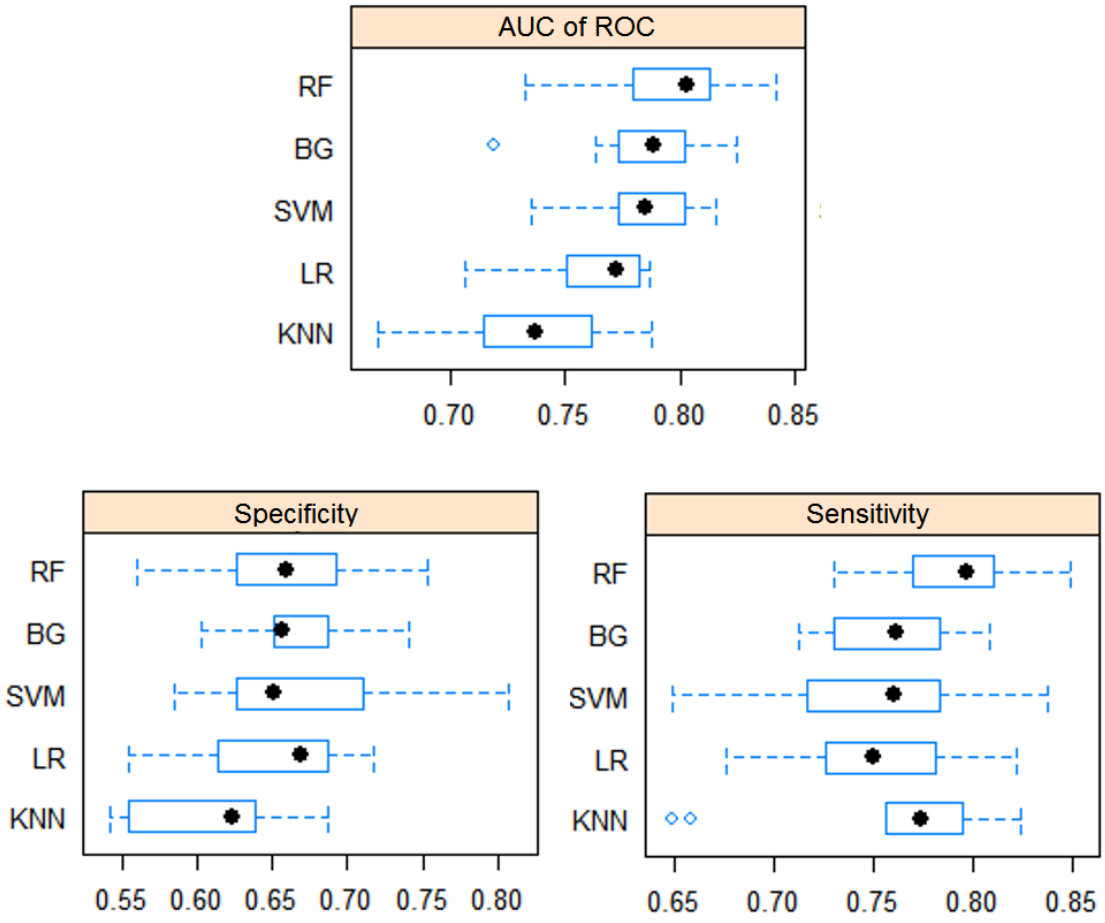

Supplementary Figure 5: Box-whisker plot showing specificity, sensitivity, and AUC of the ROC for different models during the resampling procedure. The boxes are ordered from highest to lowest mean AUC, sensitivity (TPR: ratio of true to all positives), and specificity (1-FPR, ratio of false positives to all negatives). The spread of these measures for each algorithm corresponds to repeated evaluations during the 10-fold cross-validation process.

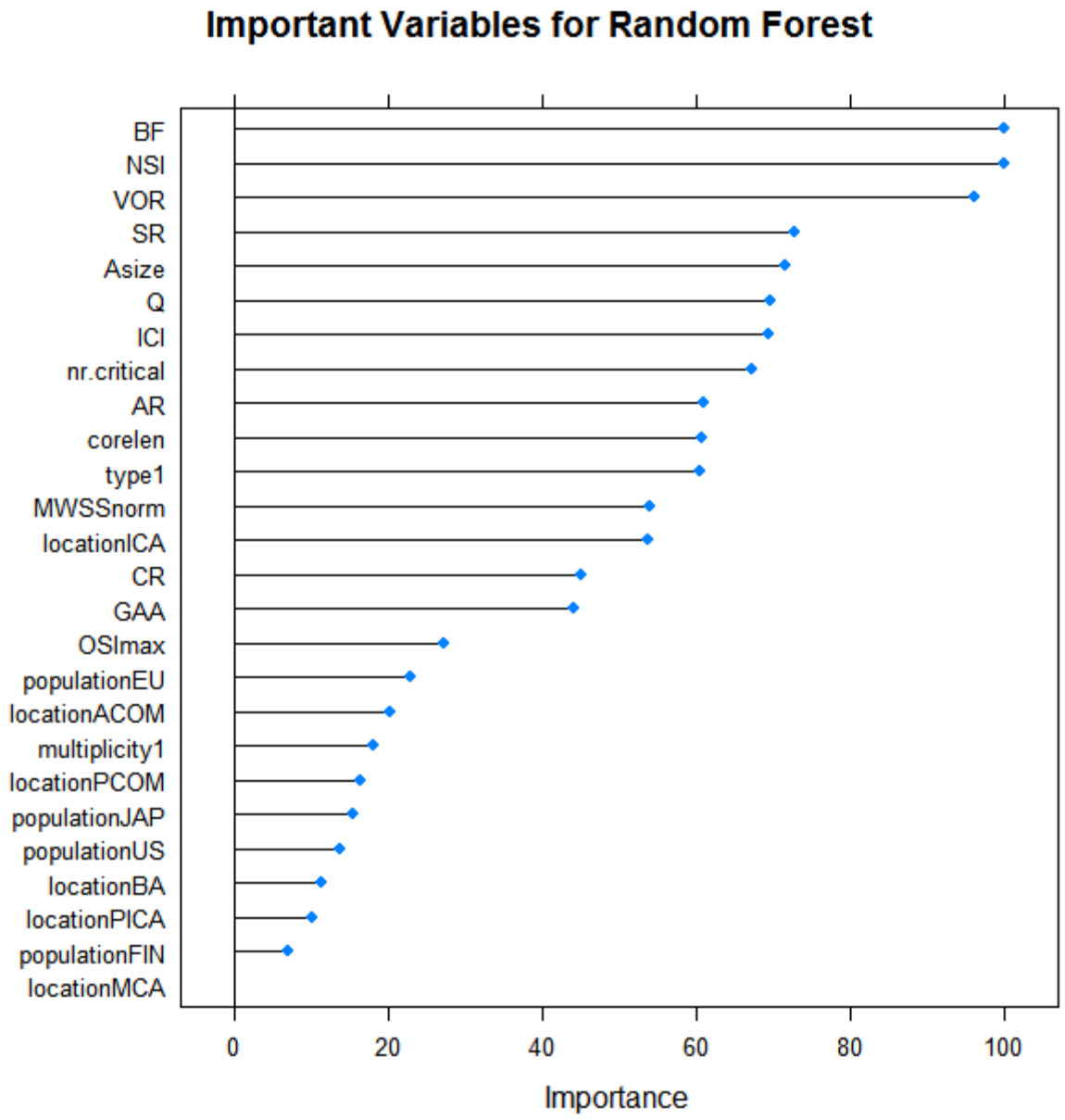

Supplementary Figure 6: Variable importance for the RF model applied to the validation dataset. Variables are ordered from top to bottom according to their importance determined by the mean decrease in Gini. The importance measures were scaled to the range 1-100 for better visualization.